Mesoscopic Quantum Coherence in an Optical Lattice

D. L. Haycock,[1] P. M. Alsing,[2] I. H. Deutsch,[2] J. Grondalski,[2] and P. S. Jessen[1]
[1]*Optical Sciences Center, University of Arizona, Tucson, Arizona 85721*
[2]*Department of Physics and Astronomy, University of New Mexico, Albuquerque, New Mexico 87131*
(Received 24 April 2000)

We observe the quantum coherent dynamics of atomic spinor wave packets in the double-well potentials of a far-off-resonance optical lattice. With appropriate initial conditions the system Rabi oscillates between the left and right localized states of the ground doublet, and at certain times the wave packet corresponds to a coherent superposition of these mesoscopically distinct quantum states. The atom/optical double-well potential is a flexible and powerful system for further study of quantum coherence, quantum control, and the quantum/classical transition.

PACS numbers: 42.50.Vk, 03.65.Bz, 32.80.Pj, 32.80.Qk

Quantum coherence between localized but separated states of a particle in a double-well potential has long served as a paradigm for nonclassical dynamics. Of particular interest is the possibility to create and manipulate coherent superpositions of mesoscopically or macroscopically distinct quantum states and to study the role played by decoherence in the emergence of classical dynamics [1]. Extending the limits of coherent control of large quantum systems is of great fundamental interest and lies at the heart of the quest for quantum computation [2]. Macroscopic quantum tunneling [3], i.e., the *incoherent* decay of a metastable quantum state along some macroscopic system coordinate, is known to occur for the phase difference of the superconducting order parameter across Josephson junctions [4] and has been seen also in the relaxation of the cooperative magnetization vector in magnetic grains [5] and of spin domains in atomic Bose-Einstein condensates (BECs) [6]. Such phenomena do not provide evidence for superpositions of macroscopically distinguishable quantum states, for which one must undertake the much harder challenge of demonstrating *coherent* dynamics on the macroscopic scale. So far, quantum coherent dynamics has been achieved only on a mesoscopic scale, notably in ion traps [7] and cavity QED [8], though spectroscopic evidence for the existence of macroscopic superpositions has very recently been seen in SQUIDs [9]. Proposals also exist to search for macroscopic quantum coherence in BECs [10].

In this Letter we report the observation of quantum coherent dynamics in a new system consisting of cesium atoms in wavelength-sized optical double-well potentials in a far-off-resonance optical lattice. The atomic wave packets undergo clear Rabi oscillations between two localized states with a mesoscopic separation of $\sim$150 nm, at frequencies that show excellent quantitative agreement with theory. Our experiment gives insight into decoherence and dephasing of delocalized wave packets in deep optical lattices and provides guidance for proposals to implement quantum logic in this system [11]. Optical lattices [12], created by the ac Stark shift in laser standing waves, are well suited for studies of quantum coherent dynamics due to low rates of decoherence and the flexibility with which the optical potential can be designed [13]. Dissipation can be engineered back into the system in a well controlled manner through noise on the potentials, photon scattering, and Raman sideband cooling [14]. Last but not least, one can hope to apply a range of quantum control techniques, including pure state preparation, controlled unitary evolution, and quantum state reconstruction. Earlier work on quantum transport in optical lattices has explored a number of related phenomena such as Bloch oscillations and Wannier-Stark ladders [15], Landau-Zener tunneling [16], and tunneling in optical gauge potentials [17]. The coherent dynamics studied in those experiments, however, involved shallow potentials and a continuum of Bloch states, rather than the discrete two-level dynamics demonstrated here.

Our atom/optical lattice system has been discussed in detail in [13], and only the most important features are summarized. The lattice is produced by two counterpropagating laser beams with linear polarizations at an angle θ (1D lin-θ-lin configuration), forming σ_+ and σ_- polarized standing waves with a relative spatial phase given by θ. It is detuned $\sim$3000Γ below the cesium $6S_{1/2}(F = 4) \rightarrow 6P_{3/2}(F = 5)$ transition, far compared to the excited-state hyperfine splitting. In this limit the lattice potential can be written in terms of a scalar potential (proportional to the field intensity) and a fictitious magnetic field (proportional to the field ellipticity) interacting with the magnetic moment $\hat{\vec{\mu}} = -g_F \mu_B \hat{\mathbf{F}}$, where $\hat{\mathbf{F}}$ is the angular momentum operator for the hyperfine state F. If we include an external magnetic field $\mathbf{B}$ the resulting potential is

$$\hat{U}(z) = U_J(z) + g_F \mu_B \hat{\mathbf{F}} \cdot \mathbf{B}_{\mathrm{eff}}(z),$$

$$U_J(z) = \frac{4U_1}{3}[1 + \cos\theta \cos(2k_L z)],$$

$$\mathbf{B}_{\mathrm{eff}}(z) = -\frac{2U_1}{3\mu_B} \sin\theta \sin(2k_L z)\mathbf{e}_z + \mathbf{B},$$

where U_1 is the light shift produced by a single lattice beam driving a transition with unit oscillator strength.

One typically defines *diabatic* and *adiabatic* potentials as the diagonal elements (in the basis $\{|m_F\rangle\}$) and eigenvalues of $\hat{U}(z)$, respectively; the former govern the motion when the internal atomic state is independent of z (e.g., in a lattice with no coupling between different $|m_F\rangle$), the latter when it adiabatically follows the direction of $\mathbf{B}_{\mathrm{eff}}(z)$ (the Born-Oppenheimer approximation). For our parameters the lowest adiabatic potential (Fig. 1) forms a periodic array of double wells. The lattice polarizations on the two sides of the well are predominantly σ_+ and σ_- and the eigenstates of $\hat{U}(z)$ in these regions have predominantly $m_F > 0$ and $m_F < 0$ character, so that motion from one side of the well to the other is accompanied by rotation of the spin. The spin thus acts as a "meter" through which one can measure the evolution of the center-of-mass atomic wave packet.

For our system the Born-Oppenheimer approximation breaks down and one cannot describe the dynamics in terms of a particle moving on the adiabatic potential. We solve instead for the *exact* energy spectrum (band structure) and stationary states of the complete lattice Hamiltonian. For the parameters of Fig. 1 the two lowest bands are split by a small energy $\hbar\Omega$, much less than the separation to the next excited bands. In addition, the negligible band curvature shows that tunneling between different double wells is unimportant. It is then possible to restrict the dynamics to a subspace spanned by the Wannier spinors $|\psi_S\rangle$ and $|\psi_A\rangle$, corresponding to the symmetric/antisymmetric ground doublet of individual double wells. We can recast the problem in familiar terms by defining left and right localized states $|\psi_L\rangle = (|\psi_S\rangle + |\psi_A\rangle)/\sqrt{2}$ and $|\psi_R\rangle = (|\psi_S\rangle - |\psi_A\rangle)/\sqrt{2}$ and see immediately that the system will Rabi oscillate between these at frequency Ω if initially prepared in, e.g., $|\psi_L\rangle$. We emphasize that $|\psi_L\rangle$ and $|\psi_R\rangle$ are *spinor* wave packets with highly entangled internal and motional degrees of freedom, whose dynamics is governed by the full lattice Hamiltonian. Figure 2 shows the spatial probability distribution (obtained by tracing over the internal state) and magnetic populations (obtained by tracing over the center-of-mass coordinate), at different times during the Rabi oscillation. Note that the key property of a double-well system is preserved: the spatial probability densities corresponding to $|\psi_L\rangle$ and $|\psi_R\rangle$ are localized on the left and right sides of the double well, and the minimal overlap between them ensures that the states can be effectively distinguished by the mesoscopic center-of-mass coordinate.

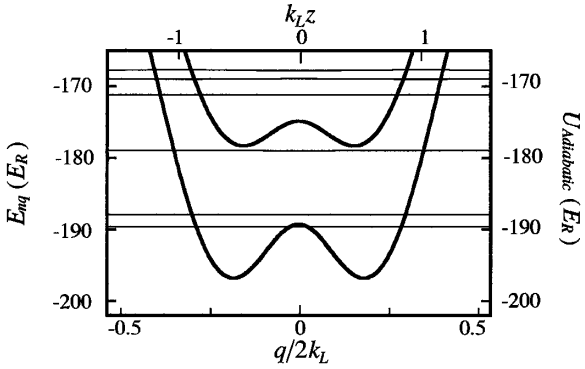

FIG. 1. Lowest two adiabatic potentials (thick curves) and six energy bands (thin lines) for $U_1 = 84E_R$, $\theta = 80°$, $B_x = 85$ mG, and $B_z = 0$ mG.

We prepare atoms in the optical lattice and follow their quantum coherent dynamics as follows. First, a standard magneto-optical trap/3D molasses is used to prepare $\sim 10^6$ cesium atoms with a temperature of $\sim 4\ \mu$K within a $\sim 200\ \mu$m rms radius. The atoms are cooled further in a near-resonance 1D lin-θ-lin lattice and then adiabatically transferred to the far-off-resonance 1D lin-θ-lin lattice. The two 1D lattices are oriented vertically, which allows us to measure the atomic momentum distributions by time-of-flight analysis, and the magnetic populations by Stern-Gerlach analysis [18]. Care is taken to assure that the lattice polarizations are linear and at the appropriate angle and that the background magnetic field is less than ~ 0.3 mG. Once in the far-off-resonance lattice the atoms are optically pumped to $m_F = 4$. We then select the motional ground state in the $m_F = 4$ potential by lowering the lattice depth until only the lowest band is bound, and accelerating the lattice at 300 m/s^2 for 1.5 ms to allow atoms in higher bands to escape [16]. The state selection is done in the presence of a large external B_z to lift degeneracies between different potentials and prevent precession

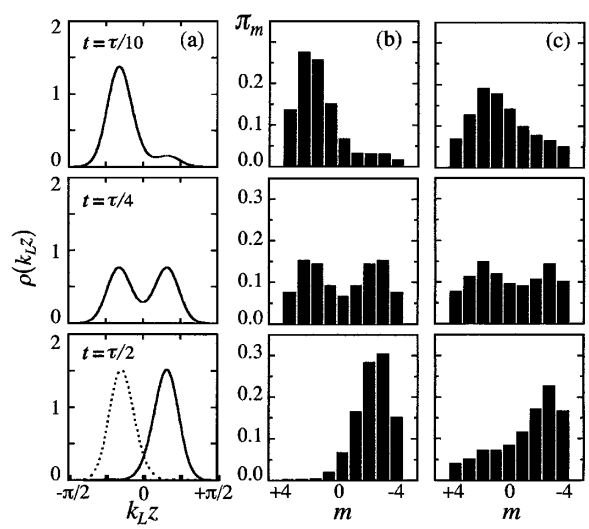

FIG. 2. Spinor wave packets during a Rabi oscillation. Parameters are identical to Fig. 1. (a) Center-of-mass probability density calculated from the Wannier states. The dotted curve in the plot for $t = \tau/2$ indicates the distribution at $t = 0$ and shows the minimal spatial overlap of the left and right localized wave packets. (b) Magnetic populations calculated from the Wannier states. (c) Experimentally measured magnetic populations. The preparation of the initial state is not instantaneous on the time scale of the Rabi oscillation and we cannot assign an effective $t = 0$ for the experiment. The first row therefore shows calculated and measured distributions at a slightly later time, $t = \tau/10$.

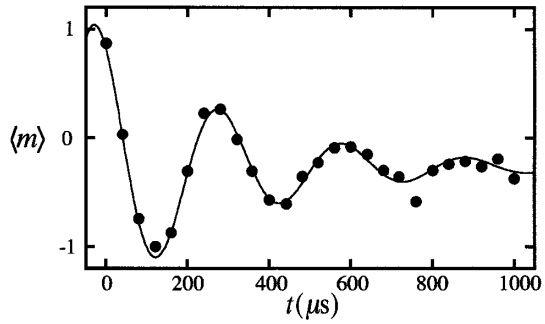

FIG. 3. Typical magnetization oscillation as a function of time, for parameters identical to Fig. 1. The solid line is a fit to a decaying sinusoid.

of the magnetic moment. When the population in higher bands has been eliminated we increase the lattice depth to the value used in the experiment and change the acceleration so that the lattice frame is in free fall. This prepares roughly 90% of the atomic population in the lowest band of the $m_F = 4$ potential, estimated from the measured momentum spread and magnetic populations. To initiate Rabi oscillations we adiabatically connect this state to a localized state in a symmetric double-well potential, by ramping B_x from zero to its desired value in 250 μs, then ramping B_z to zero in 70 μs. To create the desired localized state the final turn-off of B_z must be fast compared to the ground-doublet splitting, but slow compared to the separation from higher bands. We have checked, by numerical integration of the time-dependent Schrödinger equation using the full lattice Hamiltonian, that this requirement can be met over a wide range of parameters including those used here.

Rabi oscillations between $|\psi_L\rangle$ and $|\psi_R\rangle$ are detected by measuring the magnetic populations. Figure 3 shows a typical oscillation of the magnetization as a function of time. Our data fit well to an exponentially damped sinusoid, and we can extract good measures for the Rabi frequency over a wide range of parameters. Figures 4(a) and 4(b) show the measured frequencies versus the single beam light shift U_1 and transverse magnetic field B_x, together with the ground-doublet splitting predicted by band structure calculations. To carry out a direct theory/experiment comparison we independently measure U_1 to within $\pm 2\%$ [19] from parametric wave packet oscillations, and the external B_x to within $\pm 1\%$ from Larmor precession of the magnetic moment. Excellent agreement is observed, especially if we allow for a $\sim 4\%$ systematic underestimate of U_1. Figure 4(c) shows the variation of the Rabi frequency versus B_z, which changes the energy asymmetry (detuning) of the two-level system. The observed dependence is characteristic of two-level dynamics and confirms that our system is restricted to the ground doublet.

We have also the possibility to examine the magnetic populations in detail during the Rabi oscillation. Figure 2(c) shows typical values at $t = \tau/10$, $t = \tau/4$, and $t = \tau/2$, where $\tau = 2\pi/\Omega$ is the Rabi period. Generally, we find qualitative agreement with the results of a band structure calculation, though the experiment shows a somewhat smaller net magnetization than expected. This might indicate that the initial state is slightly mixed, with $\sim 80\%$ population in $|\psi_L\rangle$ and $\sim 20\%$ population in $|\psi_R\rangle$. There is also a slight modification of the measured populations due to a small degree of adiabatic following as we turn on a magnetic field to define the quantization axis for our Stern-Gerlach measurement. This effect is responsible for the deviation from the expected mirror symmetry of $|\psi_L\rangle$ and $|\psi_R\rangle$ around $m_F = 0$. Of particular interest is the spinor wave packet at $t = \tau/4$, where $|\psi(t)\rangle \propto |\psi_L\rangle - i|\psi_R\rangle$. Within the limits just mentioned we measure magnetic populations consistent with this delocalized superposition state, though the populations by themselves do not allow us to distinguish between a coherent superposition and an incoherent mixture of $|\psi_L\rangle$ and $|\psi_R\rangle$. Evidence of the coherence comes instead from the persistence of Rabi oscillations at later times.

As illustrated by the data in Fig. 3, we find that the amplitude of the Rabi oscillations decays with a time constant of a few hundred microseconds. We estimate the time scale for decoherence from photon scattering to be ~ 1 ms,

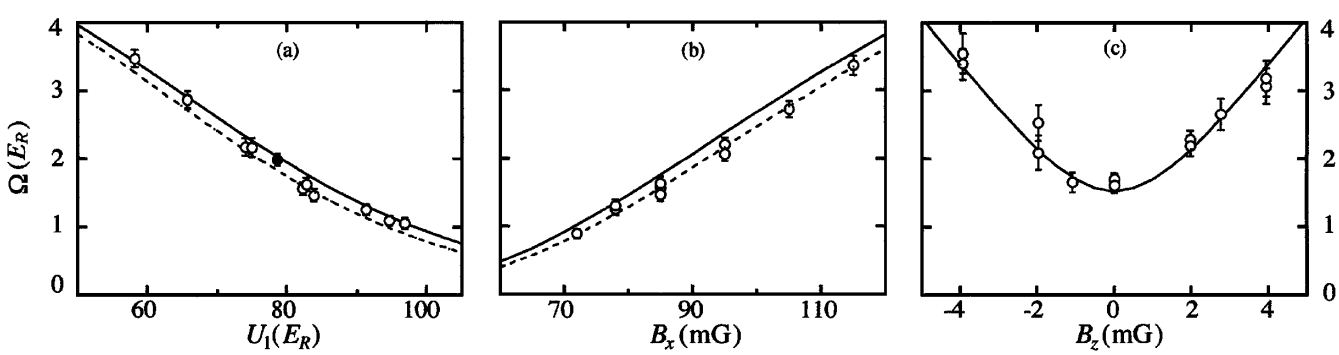

FIG. 4. Measured Rabi frequencies with base lattice parameters identical to Fig. 1, except for one parameter as indicated in the plots. (a) Ω versus U_1, (b) Ω versus B_x, and (c) Ω versus B_z. Open (filled) circles indicate data taken for a lattice tuned below (above) resonance. The solid curves show the ground-doublet splitting from band structure calculations, with no free parameters; the dashed curve shows the same splitting with a 4% increase in U_1 relative to our best independent estimate.

which is too slow to account for the observed damping. We have looked at Rabi oscillations also in a lattice tuned above atomic resonance, where the coherent dynamics is identical but the rate of photon scattering is reduced by a factor of 2 to 3. In practice we see no difference in the decay rate. This suggests that the decay is caused by dephasing of the Rabi oscillations, which occurs because different atoms see a slightly different lattice environment. The most likely cause is an estimated $\sim 5\%$ variation of the lattice beam intensities, which is consistent with the observed dephasing time. The dephasing underscores the fragile nature of highly entangled states of atomic internal and external degrees of freedom and suggests that proposals for quantum information processing [11] should seek clean separation of spin and center-of-mass motion.

In summary, we have observed Rabi oscillations of atomic spinor wave packets in the optical double-well potentials of a far-off-resonance 1D lin-θ-lin optical lattice. We have taken extensive data for a relative polarization angle $\theta = 80°$, plus additional data at $\theta = 85°$ (not shown here). Both data sets show Rabi frequencies in excellent agreement with theory. The persistence of oscillation for a few Rabi periods indicates that quantum coherent superpositions of the left and right localized states occur at certain times. Furthermore, the decay of these oscillations is most likely not caused by intrinsic decoherence from photon scattering, but rather by lattice inhomogeneity across the atomic sample. Dephasing can, in principle, be reversed by spin-echo techniques similar to those employed in nuclear magnetic resonance, and we are setting up an improved experiment to explore this possibility. With better lattice homogeneity and larger detuning and echo techniques we hope to explore coherent dynamics on time scales much longer than the Rabi period. We can then reintroduce dissipation and study the fundamental process of decoherence, as well as the transition from quantum coherent to classical dynamics. This last aspect is especially intriguing, as the coupled spin-motion Hamiltonian associated with this system can be mapped onto the Tavis-Cummings model without the rotating wave approximation, whose classical counterpart exhibits deterministic chaos [20]. Our system should then allow us to study the effects of decoherence on the emergent nonlinear behavior [21]. Additional phenomena, such as the coherent suppression of tunneling [22], can be studied in the presence of coherent driving fields.

We thank K.-I. Cheong, S. Ghose, and G. Klose for helpful discussions. P. S. J. was supported by NSF, ARO, and JSOP. I. H. D. was supported by NSF and ONR.

[1] *Decoherence and the Appearance of the Classical World in Quantum Theory,* edited by D. Giulini *et al.* (Springer, Berlin, 1996).
[2] *Introduction to Quantum Computation and Information,* edited by H.-K. Lo, S. Popescu, and T. Spiller (World Scientific, Singapore, 1998).
[3] A. O. Caldeira and A. J. Leggett, Phys. Rev. Lett. **46**, 211 (1981).
[4] J. Clarke *et al.,* Science **239**, 992 (1988).
[5] *Macroscopic Quantum Tunneling of the Magnetic Moment,* edited by E. M. Chudnovsky and J. Tejada (Cambridge University Press, Cambridge, England, 1997).
[6] D. M. Stamper-Kurn *et al.,* Phys. Rev. Lett. **83**, 661 (1999).
[7] C. Monroe *et al.,* Science **272**, 1131 (1996).
[8] M. Brune *et al.,* Phys. Rev. Lett. **77**, 4887 (1996).
[9] J. R. Friedman *et al.,* Nature (London) **406**, 43 (2000).
[10] J. I. Cirac *et al.,* Phys. Rev. A **57**, 1208 (1998).
[11] G. K. Brennen *et al.,* Phys. Rev. Lett. **82**, 1060 (1999); D. Jaksch *et al., ibid.* **82**, 1975 (1999).
[12] P. S. Jessen and I. H. Deutsch, Adv. At. Mol. Opt. Phys. **37**, 95 (1996).
[13] I. H. Deutsch and P. S. Jessen, Phys. Rev. A **57**, 1972 (1998).
[14] C. J. Myatt *et al.,* Nature (London) **403**, 269 (2000).
[15] M. Ben-Dahan *et al.,* Phys. Rev. Lett. **76**, 4508 (1996); S. R. Wilkinson *et al., ibid.* **76**, 4512 (1996).
[16] C. F. Bharucha *et al.,* Phys. Rev. A **55**, R857 (1997).
[17] S. K. Dutta, B. K. Teo, and G. Raithel, Phys. Rev. Lett. **83**, 1934 (1999).
[18] D. L. Haycock *et al.,* Phys. Rev. A **57**, R705 (1998).
[19] One standard deviation, combined statistical and systematic.
[20] P. W. Milonni, J. R. Ackerhalt, and H. W. Galbraith, Phys. Rev. Lett. **50**, 966 (1983).
[21] S. Habib, K. Shizume, and W. H. Zurek, Phys. Rev. Lett. **80**, 4361 (1998).
[22] M. Grifoni and P. Hänggi, Phys. Rep. **304**, 229 (1998).